Aghoutane *et al.*
Journal of Analytical Science and Technology (2024) 15:3
https://doi.org/10.1186/s40543-024-00417-5

Journal of Analytical Science and Technology

RESEARCH ARTICLE Open Access

Glyphosate detection via a nanomaterial-enhanced electrochemical molecularly imprinted polymer sensor

Youssra Aghoutane[1,2], Hakan Burhan[3], Fatih Sen[3*], Benachir Bouchikhi[2] and Nezha El Bari[1*]

Abstract

Glyphosate (GLY) is a widely used herbicide with an important role in agriculture. It effectively controls weeds, enhancing agricultural yield and product quality. However, its use raises significant concerns such as potential risks to non-target ecosystems and human health. In response to these concerns, we develop an electrochemical sensor with a molecularly imprinted polymer (MIP) and gold nanoparticles for GLY detection. The sensor includes a screen-printed carbon electrode (SPCE) functionalized with gold nanoparticles and a self-assembled polyvinyl carboxylic acid chloride (PVC-COOH) layer. GLY compounds interact with carboxylic groups and are encapsulated by a polymer of methacrylic acid (MAA) cross-linked with ethylene glycol dimethacrylate (EGDMA). Electrochemical performance was assessed using differential pulse voltammetry (DPV), cyclic voltammetry (CV), and electrochemical impedance spectroscopy (EIS). Morphological characterization was performed using scanning electron microscopy (SEM), Fourier transform infrared spectroscopy (FTIR), and atomic force microscopy (AFM). The sensor exhibits impressive selectivity, detecting GLY within a range of 273–1200 pg/mL with minimal interference from other pesticides. It boasts a low detection limit of 0.8 pg/mL (signal-to-noise ratio $S/N = 3$) by DPV and 0.001 pg/mL by EIS. The sensor's versatility extends to various sample types, including surface water, agricultural wastewater, soil, and cucumber, demonstrating high recovery rates (> 96.05%) and low relative standard deviation (RSD) (< 5.7%). The developed MIP sensor is proven to be a valuable tool for rapid and highly sensitive detection of GLY in diverse environmental and agri-food samples.

Keywords Glyphosate, Gold nanoparticles, Molecularly imprinted polymer, Screen-printed carbon electrode, Agricultural wastewater, Cucumber

Introduction

Glyphosate (GLY) is a widely used non-selective herbicide that targets parasitic weeds and protects agricultural and horticultural crops (Lares et al. 2022). The main drawback of this pesticide is its persistence in ecosystems, including aquatic environments near the application areas. The environmental half-life of GLY is approximately 4 ± 2 months (Cederlund 2022). Studies have shown an increase in GLY concentrations in the environment due to its excessive use. This has harmful effects on non-target animal species, including liver and kidney damage, endocrine disruption, neurotoxicity, chromosomal aberrations and DNA damage in higher vertebrates (Gandhi et al. 2021; Lanzarin et al. 2022).

*Correspondence:
Fatih Sen
fatihsen1980@gmail.com
Nezha El Bari
nezhaelbari6@gmail.com
[1] Biosensors and Nanotechnology Group, Department of Biology, Faculty of Sciences, Moulay Ismaïl University, B.P. 11201, Zitoune, Meknes, Morocco
[2] Biosensors and Nanotechnology Group, Department of Physics, Faculty of Sciences, Moulay Ismaïl University of Meknes, B.P. 11201, Zitoune, Meknes, Morocco
[3] Sen Research Group, Department of Biochemistry, Kutahya Dumlupinar University, 43000 Kutahya, Turkey

GLY traces have been detected in cereals, foods, vegetables, and fruits, raising concerns about its impact on human health. The Food and Agriculture Organization of the United Nations (FAO) has acknowledged the potential toxicological risks associated with GLY residues accumulating in the food chain (Bou-Mitri et al. 2022; Melton et al. 2019; Xu et al. 2019). As a result, the US Environmental Protection Agency (EPA) in Europe has proposed a chronic reference dose (RfD) for glyphosate or acceptable daily intake (ADI) of 1.0 mg/kg/day (Blanco-López et al. 2003).

GLY can enter the human body through contaminated agricultural products or inhalation during spray application (Bukowska et al. 2022). Studies have detected the presence of GLY in the urine, blood, maternal serum and breast milk of people indirectly exposed to significant quantities of GLY (Campbell et al. 2022; Bus 2015; Gillezeau et al. 2019; Weisenburger 2021). Adverse effects on human health have been observed, including miscarriage, reduced fertility, thyroid disease, cardiopulmonary and muscular disorders. Neural disorders, neoplasia, and fetotoxic effects are also observed (Kalofiri et al. 2021; Kronberg et al. 2021; Maddalon et al. 2021; Madani and Carpenter 2022; Soares et al. 2021). Given the widespread use of GLY and its toxicity, the detection of GLY residues in environmental and food products is crucial to guarantee not only environmental quality but also food quality. However, conventional methods for GLY residues detection face difficulties linked to its ionic nature, low volatility, high solubility in water, insolubility in organic solvents and low molar mass (Kodama et al. 2008). Therefore, there is a need to develop new strategies that are rapid, easy, selective, and highly sensitive for the detection of GLY residues.

These classical methods include gas chromatography (GC), high-performance liquid chromatography (HPLC), capillary electrophoresis, spectrophotometry, Nuclear magnetic resonance spectroscopy (NMR), diffuse reflectance spectroscopy, and fluorescence resonance energy transfer (FRET) between carbon spots (Hori et al. 2003; Motojyuku et al. 2008; Jiang and Lucy 2007; Silva et al. 2011; Yuan et al. 2017). Although these techniques provide quantitative information, they can be complex, costly and require qualified personnel (Diouf et al. 2020). It is therefore necessary to find rapid and practical alternative methods. Electrochemical detection offers the advantage of analysing compounds on site, and has shown promise for rapid, accurate detection (Aghoutane et al. 2020; Sekli Belaïdi et al. 2019). Electrochemical sensors including luminescence sensors, aerodynamic sensors, fluorescence sensors and photoelectrochemical sensors have been investigated for the determination of many molecular structures such as GLY (Arikan et al. 2022; Akin et al. 2022; Liu et al. 2020; Li et al. 2016; Bayat et al. 2023). Recently, molecularly imprinted polymers (MIPs) have emerged as a driving force in the development of electrochemical sensors. MIPs provide high selectivity, sensitivity, low cost, ease of use, and reliability (Cao et al. 2019). They work by selectively recognizing a specific target through cavities embedded in the polymer matrix, which are created through a manufacturing process involving functional monomer pre-polymerization, cross-linking, and removal of the analyte. The resultant cavities, which are identical to the analyte in terms of size, shape, and functional group arrangement, serve as extremely selective receptors (Do et al. 2015).

However, successful preparation of various molecularly imprinted polymers (MIPs) has been achieved using methacrylic acid (MAA) (Chen et al. 2016; Tarannum et al. 2023) to specifically interact with phosphate ions and phosphonic acid groups. MIPs based on MAA have demonstrated high effectiveness in selectively binding phosphonate derivatives in organic samples or under controlled pH conditions. It is worth mentioning that MIPs utilizing MAA as a monomer have been synthesized and applied successfully for analytes containing primary or secondary amine functionalities (Cui et al. 2023).

In fact, this approach is being considered for the development of a dedicated MIP sensor for the detection of GLY, which possesses an amine functionality.

Ensuring polymer stability in the electrochemical cell over time is a challenge for some polymer-modified electrodes (Oliveira et al. 2023). Therefore, polymer stability plays a crucial role in the fabrication of polymer films for electrochemical sensors. Polymer assemblies have emerged as important components in sensor design. By selecting a host polymer with excellent mechanical stability and combining it with another polymer that functions as the chemically active part interacting with the target analyte, a robust and reliable sensor platform can be achieved (Blanco-López et al. 2003).

Polyvinyl chloride (PVC) is an attractive support material that offers excellent stability for electrochemical molecularly imprinted polymer (MIP) sensors over extended periods of time (Ngai et al. 2016).

This synthetic polymer, known for its non-toxic nature, possesses distinctive features such as flexible molecular chains, chemical stability, and a suitable matrix for application in electrochemical sensors.

In recent times, screen-printed electrodes (SPEs) have gained popularity as a platform for MIP-based sensors due to their ability to address memory effects and simplify the cumbersome cleaning process associated with conventional electrodes. SPEs are characterized by their rapid response, affordability, and user-friendliness. These

advantages enable on-site analysis while minimizing sample volume requirements.

Moreover, noble metals have been extensively utilized in the fabrication of electrochemical sensors to enhance their sensitivity. Metal nanoparticles, such as gold nanoparticles (AuNPs), are particularly interesting as catalysts in electrochemical applications. AuNPs possess a high specific surface area, excellent conductivity, and can be immobilized on the electrode surface to improve the mechanical and electrical properties of modified electrodes (Blanco-López et al. 2004).

Of these properties, conductivity stands out as one of the most remarkable features of these nanoparticles, significantly enhancing the electron transfer rate between the analyte's active centres and the sensor surface.

A comprehensive review of the literature indicates that this is the first instance of preparing an MIP sensor by immobilizing MAA on a screen-printed carbon electrode for the determination of GLY in various samples, including agricultural and surface wastewater, cucumber samples, and agricultural soils.

This novel electrochemical sensor offers cost-effectiveness, selectivity, and high sensitivity. The synthesis process of the MIP electrochemical sensor is evaluated using techniques such as cyclic voltammetry (CV), differential pulse voltammetry (DPV), and electrochemical impedance spectroscopy (EIS). The surface morphology of the electrodes is examined through atomic force microscopy (AFM), scanning electron microscopy (SEM), and Fourier transform infrared spectroscopy (FTIR). The fabrication process and practical application of the GLY sensor, along with its analytical properties, will be thoroughly investigated.

Materials and methods

Reagents and solutions

The following used chemicals and solutions were obtained from Sigma Aldrich: glyphosate (360 g/L), chlorpyrifos (480 g/L), carbendazim (500 g/L), polyvinyl carboxylic chloride (PVC-COOH), N'-hydroxysuccinimide (NHS), 1,4-dioxane (99.8%), phosphate buffered saline (PBS), gold (III) chloride trihydrate ($HAuCl_4 \cdot 2H_2O$) (99.99%) and trisodium citrate. Potassium ferricyanide $K_3[Fe(CN)_6]$, potassium ferrocyanide $K_4[Fe(CN)_6]$ and carbodiimide hydrochloride (EDC) were obtained from Fluka. A PBS solution (0.01 M, pH 7.0) was prepared by dissolving a PBS pellet in 200 mL of distilled water (DW). All experimental procedures were carried out in a laminar flow hood.

Apparatus

The MIP electrochemical sensor was constructed using a screen-printed carbon electrode (SPCE) purchased from DropSens, Spain. The sensor consisted of a three-electrode system: a carbon working electrode, a silver reference electrode and a carbon counter electrode.

AFM analysis was performed in tapping mode using a nanomagnetic instrument device with a maximum resolution of 256 µm in a scan area of 10 µm × 15 µm. AFM images were processed using the hpspm 1.11 Beta software provided by NMI.

Fourier transform infrared (FTIR) spectroscopy spectra were acquired using a PerkinElmer Spectrum Two FTIR spectrometer, operating at a resolution of 4 cm^{-1} over a wavenumber range of 500–4000 cm^{-1}. All spectra were recorded at room temperature after averaging four scans.

For scanning electron microscope (SEM) analysis, a DPU-ILTEM instrument was used, operating at an accelerating voltage of 15 kV and a magnification of ×50,000. The same equipment was used for energy-dispersive X-ray spectroscopy (EDS) to study the chemical composition in conjunction with the SEM.

Synthesis of MIP, and NIP materials on the carbon electrode

To prepare the screen-printed carbon electrodes (SPCE) for deposition, a cleaning process was performed. The electrodes were initially washed with 99.8% ethanol and then rinsed with distilled water (Rong et al. 2015).

The functionalization of the SPCE involved the use of gold nanoparticles (AuNPs) and a layer of polyvinyl carboxylic acid chloride (PVC-COOH). The PVC-COOH was dissolved in 1.4-dioxane at 40 °C to increase its melting point through intermolecular interactions. A 5 µL solution of PVC-COOH (11 mg/1.25 mL dioxane) was deposited on the working SPCE and incubated at room temperature for 90 min. Subsequently, the unreacted EDC and NHS molecules were thoroughly rinsed off with distilled water (Bakas et al. 2012).

To immobilize GLY, 3.5 µL of a GLY solution (0.1 mmol) was applied to the surface of the SCPE/PVC-COOH and incubated for 2 h. The SPCE was then washed twice with a PBS buffer solution at pH 7.4 to remove any unbound GLY compounds.

For the pre-polymerization step, a solution was prepared by mixing MAA (2 mM) as the functional monomer and ethylene glycol EGDMA (1 mM) as the cross-linking agent in 10 mL of acetonitrile solvent. The solution was thoroughly mixed with a magnetic stirrer for 1 h. Subsequently, 3 µL of the resulting solution was deposited onto the surface of the working electrode.

The polymerization process was carried out at a temperature of 45 °C for 12 h. This temperature was chosen as MIP materials tend to swell at this temperature, facilitating the penetration of the target molecules into the material (Diouf et al. 2017; Zhao et al. 2015).

Furthermore, obtaining a rapid and accurate determination of the analyte is highly dependent on the optimization of the GLY extraction step. The extraction step is a crucial factor in the preparation of MIPs since high levels of purification can be achieved by optimizing the time of template-selective extraction and the volume of solvent used. In this study, the extraction step time and solvent volume were optimized to improve GLY binding. Specifically, a mixture of methanol and acetic acid (9:1 (v/v)) was used to extract the printed molecule for 20 min. This created free sites on the surface of the electrode that allowed the recognition of GLY at different concentrations.

A sensor based on a non-printed polymer (SPCE/NIP) was prepared using the same procedure, but without adding the target molecule to the polymer solution. The aim of this control test is to verify that the effects observed in the MIP detection were only due to the existence of memory sites.

Preparation of samples

Agricultural wastewater, samples of agricultural wastewater, surface water, cucumber, and soil were collected from the same agricultural region in Meknes, with approximately 150 m between each sampling site. Prior to analysis, water samples were mixed and filtered through 0.45 µm membrane filters. A 50 µL volume of the filtered water samples was then applied to the MIP sensor for analysis.

For cucumber samples, 200 g of the samples were homogenized using a food blender. Then, 50 g of the homogenized sample were immersed in 50 mL of acetonitrile solution. The mixture was incubated on a water bath oscillator at a temperature of 20 °C for 5 h. After incubation, the mixture was centrifuged, and the supernatant was collected. The sediment at the bottom of the centrifuge tube was washed multiple times with acetonitrile. The supernatant and washes collected were concentrated using a rotary evaporator, and the residue obtained was dissolved again in 20 mL acetonitrile to obtain the spiked sample solution.

The soil samples were extracted according to the following procedure. At the first, 10 g of homogenized dried soil were shaken with 20 mL of 0.6 M KOH for 30 min. The mixture was then centrifuged, and the supernatant was filtered through a 0.22 µm membrane filter (Li et al. 2009).

Additionally, a tap water sample without GLY contamination was collected from the laboratory. This tap water sample was divided into three aliquots, each spiked with different concentrations of GLY (273, 355, and 533 pg/mL). After thorough mixing, a volume of 50 µL from each spiked aliquot was deposited onto the working electrode. The standard addition method was employed to analyse the tap water samples, ensuring accurate results.

Molecular imprinting process

The electrochemical properties of the MIP sensor's production process were investigated in a solution of $[Fe(CN)_6]^{3-/4-}$containing PBS (pH = 7.2) at 5 mM. The $[Fe(CN)_6]^{3-/4-}$ redox probe was chosen as a marker to examine changes in the electrode surface after each step of sensor preparation. The procedure for preparing the MIP sensor is shown in Scheme 1. The entire process can be summarized in the following steps: Firstly, the 0.1 mM GLY (matrix) solution with was deposited on the surface of the SCPE/AuNPs/PVC-COOH for 4 h. Secondly, the polymer solution containing 2 mM MAA (functional monomer) and 1 Mm EGDMA (cross-linking monomer) was deposited on the surface of the working electrodes. In the third step, polymerisation was carried out for 12 h in the oven at 45 °C. Finally, the target molecule was extracted using a solution of methanol, and acetic acid (9:1 (v/v)). The electrochemical detection of the GLY by the MIP sensor was carried out by placing 30 µL of each GLY concentration on the working electrode for 30 min. The electrochemical measurements were carried out in the presence of a solution of $[Fe(CN)_6]^{3-/4-}$ as a redox probe.

Spectroscopic measurements

To analyse the changes in surface morphology and elemental composition of the modified SPCE, various techniques were employed. The AFM analysis was carried out in "tapping" mode, using a nanomagnetic instrument with a maximum resolution of 256 µm and a scanning area of 10 µm/15 µm. The NMI's hpspm 1.11 Beta software was utilized to process the AFM images. The surface changes were also examined using scanning electron microscopy (SEM) with an acceleration voltage of 15 kV and a magnification of 50000×, and the chemical composition was analysed by EDS, which was performed using the same equipment as the SEM. Additionally, the FTIR spectra were obtained using a PerkinElmer Spectrometer Spectra two, over a range of 500–4000 cm^{-1}, at a resolution of 4 cm^{-1} after an average of four scans. All spectra were obtained at room temperature.

Electrochemical measurements

All electrochemical measurements were performed using a portable instrument called PalmSens3 from Spain which was connected to a computer. The screen-printed carbon electrodes used in the experiment were purchased from DropSens. They consisted of three electrodes, a working electrode measuring 0.19 cm^2, a

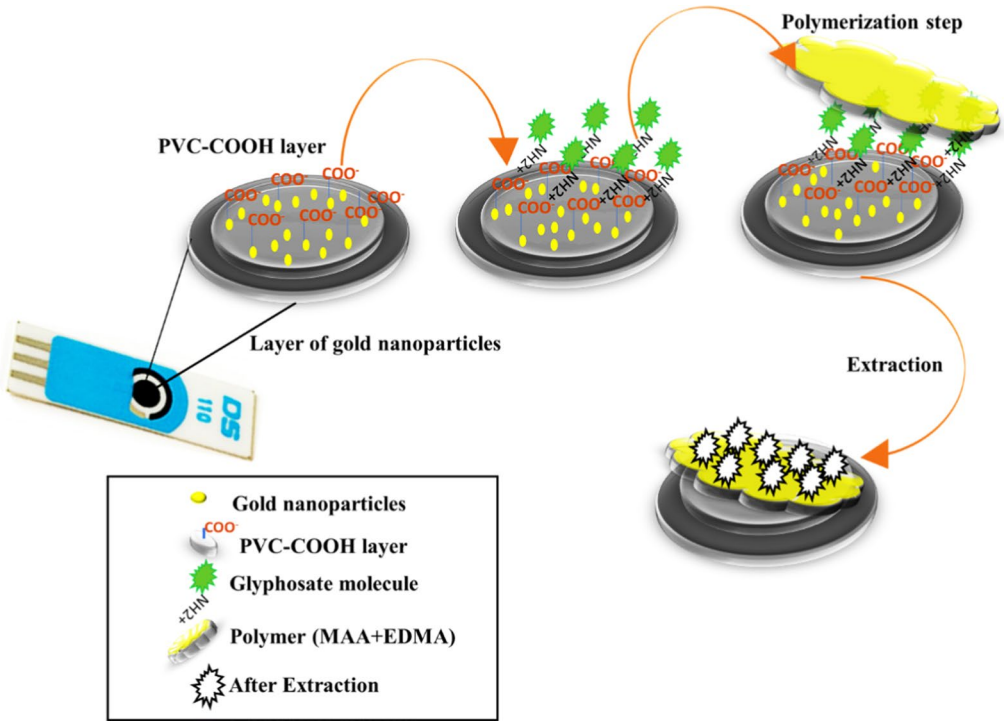

Scheme 1 Presentation of the different stages of the MIP sensor fabrication

saturated Ag reference electrode measuring 0.54 cm^2 and a carbon plate counter electrode measuring 0.54 cm^2. To measure changes in current and resistance during the development and detection phases, three different electrochemical techniques were used: cyclic voltammetry (CV), differential pulse voltammetry (DPV), and electrochemical impedance spectroscopy (EIS). DPV measurements were conducted by scanning the potential from −0.1 to 0.2 V with a scanning rate of 50 mV/s. The EIS analysis was performed at a bias potential of 10 mV, covering a frequency range of 0.1 Hz–50 kHz, and the impedance data were adjusted using the Randles equivalent circuit of 0.1 Hz–50 kHz. The impedance data were properly adjusted using the Randles equivalent circuit.

Results and discussion

Polymerization of GLY imprinted films

Upon deposition on SPCE, the mixture of MAA and GLY underwent polymerization by means of a reaction involving MAA and GLY. To investigate the alterations on the SPCE surfaces (Bare Carbon, after polymerization, and extraction), CV was employed for further characterization in a 5 mM $[Fe(CN)_6]^{3-/4-}$ solution. The CV analysis was conducted within a potential range of −0.4 to 0.6 V at a scan rate of 20 mV/s. The outcomes obtained from this analysis are illustrated in Fig. 1a, revealing the recorded

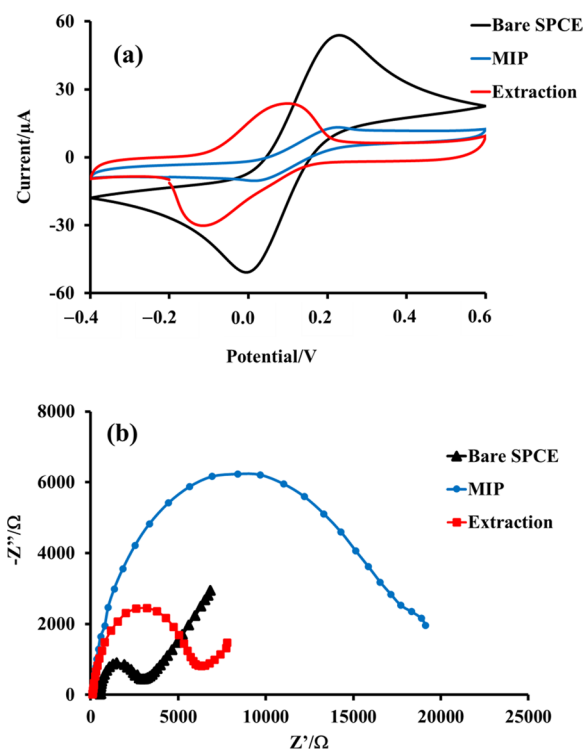

Fig. 1 Electrochemical behaviour represented as **a** Cyclic voltammograms, **b** Nyquist plots of 5 mM $[Fe(CN)_6]^{3-/4-}$ solution at Bare SPCE, SPCE/MIP and SPCE/Extraction

values for peak anode current (*I*pa) and potential (*E*pa). It is evident that the CV signal of the bare carbon electrode (*I*pa = 0.25 µA, and *E*pa = 53.09 V) surpasses that of the MIP current (*I*pa = 0.20 µA, and *E*pa = 22 V). This discrepancy suggests the successful entrapment of GLY onto the SPCE electrodes, thereby impeding the diffusion of $[Fe(CN)_6]^{3-/4-}$ to the SPCE surface. Additionally, during the extraction step, the peak current (Ipa = 0.21 µA, and Epa = 32 V) increases due to the absence of GLY molecules within the polymer matrix.

Impedance spectroscopy was also used to characterize the development steps of MIP sensor (Fig. 1b). The figure clearly demonstrates that the impedance measurements align well with the CV results, as evidenced by the correlation between the diameter of the semicircles in the Nyquist diagrams and the variations in current peaks.

Morpho-chemical characteristics of MIPs

To examine the morphology and chemical composition of the MIP sensor during its preparation, AFM and SEM measurements were carried out. Figure 2 presents three-dimensional AFM images at different stages: the bare SPCE electrode, after polymer deposition, and after GLY extraction. Prior to GLY/MAA deposition and following template extraction, AFM characterizations were performed to assess surface homogeneity and roughness of the electrode surfaces. Initially, the bare SPCE substrate exhibited a root main square (Rq) surface roughness of (*R*q = 1.04 µm) (Fig. 2a). After GLY/MAA deposition, the surface roughness increased to (*R*q = 3.54 µm) (Fig. 2b). Upon extraction, the AFM image displayed a distinct surface arrangement with extensive coverage of the electrode surface while maintaining a uniform appearance of the template. Consequently, when GLY molecules were removed from the imprinted film, the roughness decreased to (*R*q = 1.17 µm) (Fig. 2c). These obtained images validate the formation of the polymer on the electrodes and demonstrate the expected rise in surface roughness following the polymer deposition step. Furthermore, the decrease in roughness signifies the successful extraction of GLY from the MIP matrix.

These results are consistent with the electrochemical analyses as described above.

The SEM analysis of the Bare-SPCE (Fig. 3a) displayed a rough yet uniform surface. Following the modification with the GLY/polymer complex, the surface of the Au-SPE/MIP electrode exhibited a rougher thin film with a granular morphology, indicating successful deposition of the polymer onto the electrode (Fig. 3b). Conversely, the image corresponding to the extraction phase demonstrated a more compact morphology with a relatively smooth surface, featuring a layered structure and some holes (Fig. 3c). These results provide confirmation of the

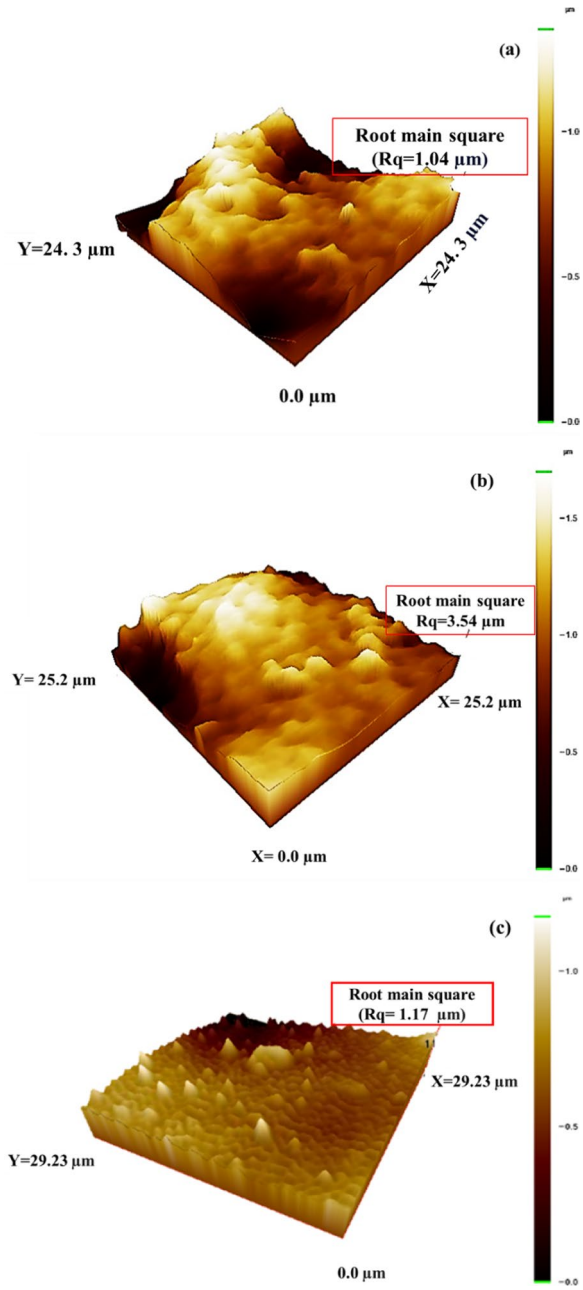

Fig. 2 AFM images of **a** Bare SPCE, **b** SPCE/MIP before extraction and **c** SPCE/MIP after extraction

preparation of the imprinted electrochemical sensor and the subsequent extraction of GLY.

The EDS spectra of the Bare-SPCE (Fig. 3a) revealed a higher presence of carbon (C) at 59.72%. After the deposition of the GLY/polymer complex, Fig. 3b exhibits peaks attributed to carbon (C) and oxygen (O) at approximately 16.72% and 3.67%, respectively, confirming the successful imprinting of GLY within the polymer.

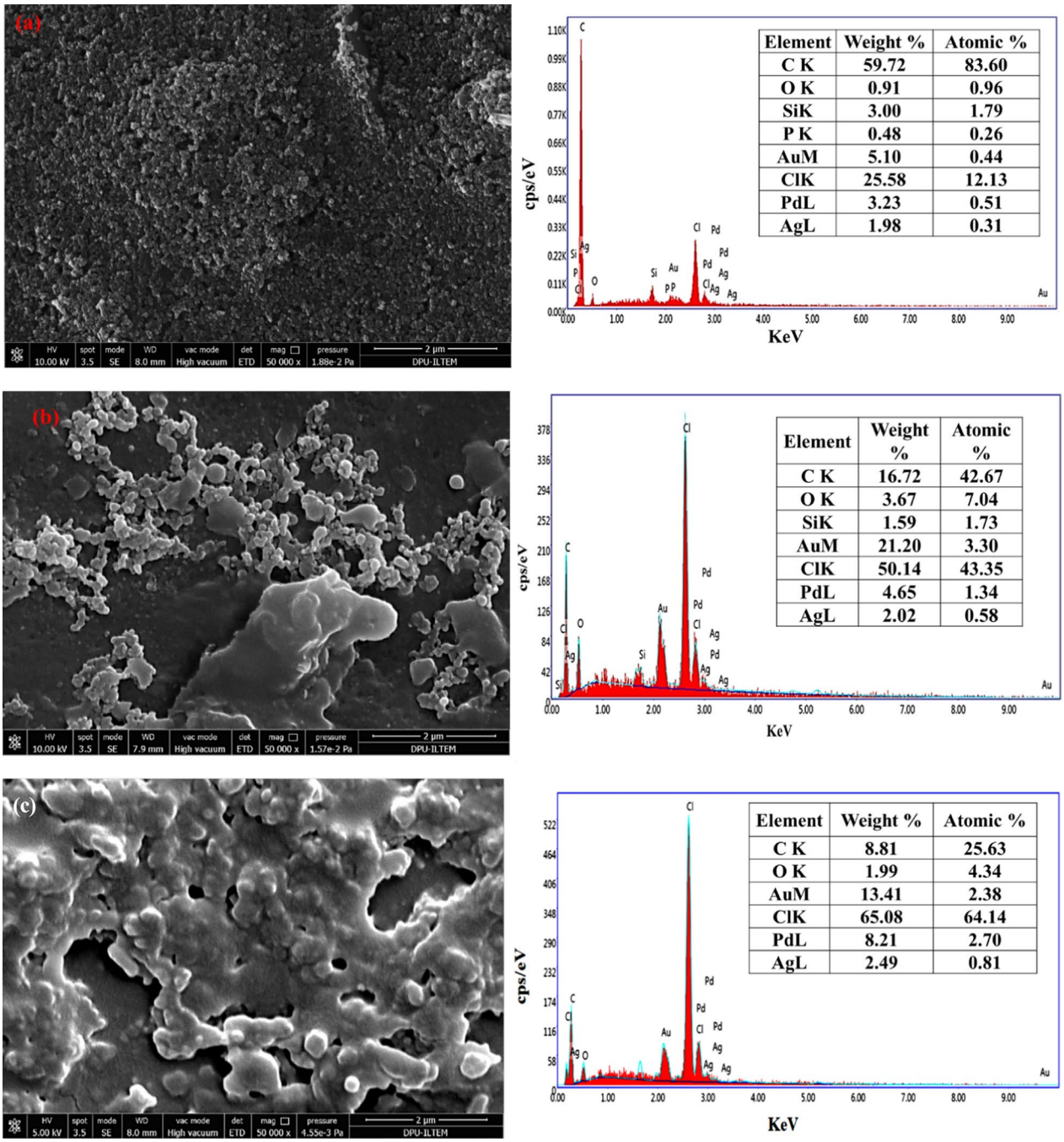

Fig. 3 SEM images of **a** Bare SPCE, **b** SPCE/MIP before extraction and **c** SPCE/MIP after extraction

Moreover, the oxygen content increased significantly after the polymerization process, which can be attributed to the presence of GLY molecules. Subsequently, during the extraction stage (Fig. 3c), a much lower oxygen content (1.9%) and carbon content (8.81%) were observed, indicating the removal of a majority of GLY molecules from the MIP matrix.

FTIR analysis was used to assess molecular interactions at the surface of the SPCE. Figure 4 shows the FTIR spectra of the bare SPCE, the SPCE/MIP and the SPCE/Extraction. In the spectrum of the SPCE/MIP sample, a notable transmittance peak centred at 1171 and 1084 cm^{-1} is evident, corresponding to the stretching band of the P–OH group found in the GLY structure

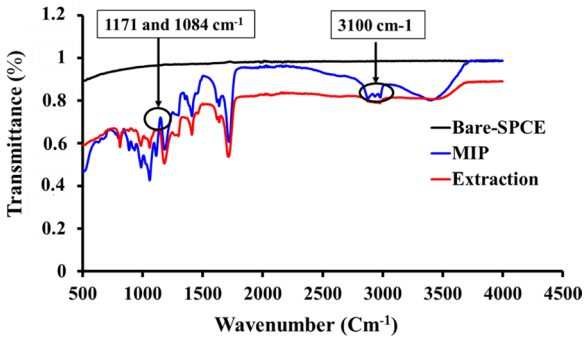

Fig. 4 FTIR spectra of SPCE, SPCE/MIP and SPCE/MIP after extraction

(Sanchez Martín et al. 1999). In addition, a small peak is observed around 3100 cm^{-1}, typically associated with the stretching vibrations of the O–H and N–H groups in GLY (Clermont-Paquette et al. 2023). In contrast, the absence of these peaks in the SPCE and SPCE/Extraction spectra indicates that the attachment of the GLY molecule on the SPCE is successful. This observation confirms the efficiency of the immobilization of the template (GLY) during the preparation of the MIP and the correct execution of the extraction step.

Molecular recognition by MIP and NIP sensors

DPV and EIS techniques were used to evaluate the sensor's retention capability for different concentrations of GLY. Figure 5a displays responses of the MIP sensor using DPV over a concentration range of 273 pg/mL to 1200 pg/mL. During the electrochemical characterization process, $[Fe(CN)_6]^{3-/4-}$ served as a mediator between the imprinted electrodes and the standard solutions. As shown in Fig. 5, the redox current peaks decrease as the GLY concentrations increase. This observation can be attributed to the dense film that covers the surface of the SPCE electrode, confirming the binding of GLY molecules and hindering the electron transport of the $[Fe(CN)_6]^{3-/4-}$ redox probe.

Figure 5b illustrates the Nyquist plots corresponding to the detection of different GLY concentrations. These plots provide information about the interfacial charge-transfer resistance (Rct), which was determined from the diameter of the semicircles using Z-spectrum software for better fitting. The semicircles on the Nyquist graph expand as the GLY concentrations increase. This increase in GLY concentration leads to a higher resistance to charge transfer, which can be explained by the filling of specific cavities with GLY molecules.

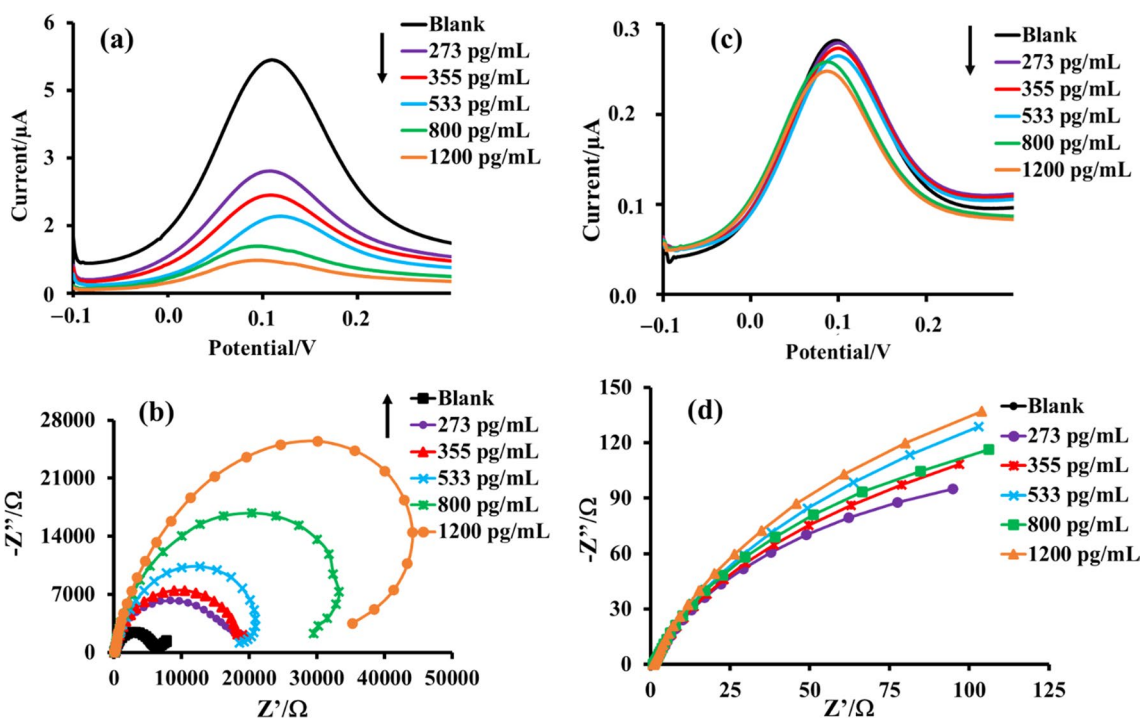

Fig. 5 Electrochemical responses of the MIP sensor with the increasing concentration of Glyphosate obtained by DPV: **a** MIP, **c** NIP, and EIS: **b** MIP, **d** NIP in a PBS electrolyte containing 5 mM $[Fe(CN)_6]^{3-/4-}$as redox probe

In contrast, when analysing the non-imprinted polymer (NIP) data obtained under the same conditions, the current peaks show negligible variation (Fig. 5c). This is likely due to the absence of GLY during the polymerization process, resulting in absence of specific cavity creation. Moreover, the Nyquist diagrams of the NIP sensor show linear plots without any semi-circular patterns and negligible changes in resistance values (Fig. 5d). These results suggest that the NIP sensor has no specificity for GLY molecules, asserting that the responses observed in the MIP sensor result exclusively from the presence of GLY cavities.

Calibration curve and detection limit

The GLY MIP sensor was developed using the optimal conditions and parameters described above. The sensor was exposed to different concentrations of GLY ranging from 273 to 1200 pg/mL. DPV method was employed within the voltage range of −0.1 to 0.3 V to observe the sensor responses. The maximum response values were used to construct the calibration curves. A logarithmic relationship between MIP sensor responses and Log GLY concentrations was observed, resulting in the equation $Y = -3.39\ \mathrm{Log}(C) + 10.24$ with an R^2 value of 0.97.

The linear correlation between current peaks and corresponding concentrations is depicted in Fig. 6, where the calibration curves of the MIP (Fig. 6a) and NIP (Fig. 6b) sensors show the relative variation of $I{-}I_0/I_0$ as a function of the logarithmic GLY concentrations. Each data point on the calibration curve represents the average of three replicates. The calibration curve for the MIP has a good linearity coefficient of 0.97 and a slope of −3.4. This shows that as the GLY concentrations are increased, the MIP sensor responds well and linearly. On the other hand, the NIP sensor generates almost constant relative responses (between −0.12 and 0), hence the poor linearity.

Figure 6 also shows the calibration curve for the sensor responses obtained using the EIS technique. The value of $\Delta R/R_0$ was calculated for each GLY concentration. In addition, the normalized data for the MIP sensor showed a notable slope accompanied by a linearity coefficient of 0.93 (Fig. 6c). In contrast, responses with no significant variation and a minimum linearity of 0.09 were obtained in the NIP test (Fig. 6d).

These results confirm that the NIP sensor was not specific to GLY molecules, demonstrating that the responses of the MIP sensor resulted solely from the presence of GLY-specific cavities.

The detection limit (LOD) and quantification limit (LOQ) were calculated using the following formula:

$$\mathrm{LOD} = k_{\mathrm{iLOD}} * \sigma / m \quad (1)$$

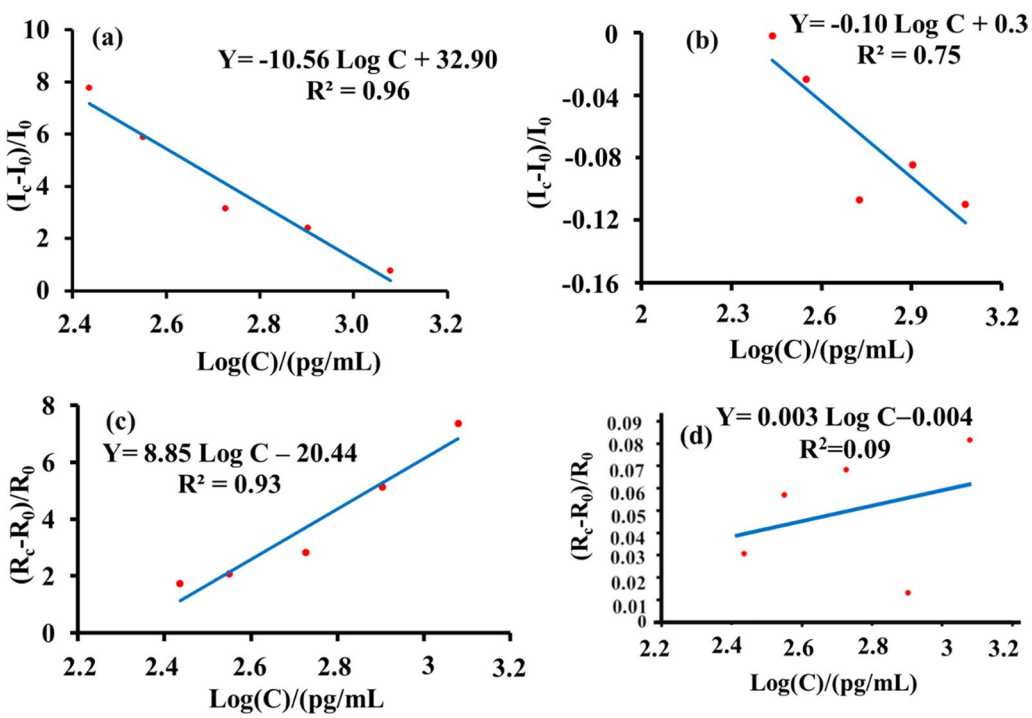

Fig. 6 Calibration curves using DPV techniques: **a** MIP, **b** NIP sensors, and EIS techniques: **c** MIP, **d** NIP sensors

Table 1 Comparison of performance between reported works and the current GLY MIP sensor

Methods for GLY detection	LOD pg/mL	References
Colorimetric immunosensor	20	Şengül (2016)
Electrochemical sensor based on molecularly imprinted polypyrrole nanotubes	1940	Zhang et al. (2017)
Electrochemical impedance spectroscopy determination of glyphosate using a molecularly imprinted chitosan	0.001	Xu et al. (2017)
Polypyrrole molecularly imprinted polymer	920	Ding et al. (2021)
Electrochemical sensor based on a gold electrode modified with a molecularly imprinted polypyrrole	270	Campanile et al. (2023)
Electrochemical MIP sensor	0.001	This work

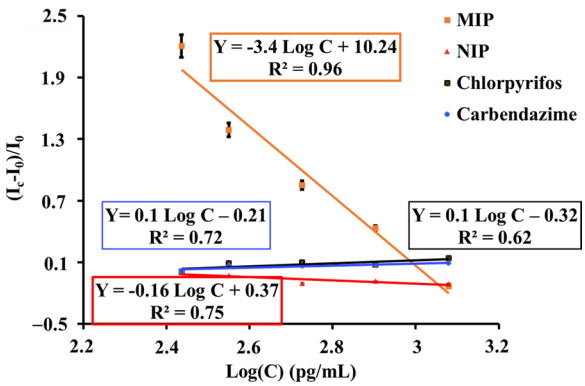

Fig. 7 Comparison of calibration curves of Glyphosate, NIP, and the interfering molecules (carbendazim and chlorpyrifos) obtained by DPV

$$\mathrm{LOQ} = k_{\mathrm{iLOQ}} * \sigma / m \tag{2}$$

where k_i represents the signal-to-noise ratio, with $k_i = 3.3$ for LOD and $k_i = 10$ for LOQ. The standard deviation of the intercept is denoted by σ, and m represents the slope (Sheals et al. 2003). For the DPV method, the LOD was found to be 0.8 pg/mL, while for EIS, it was determined to be 0.001 pg/mL. These values indicate the high detectability of the proposed method.

Comparing the analytical performance of the MIP sensor to previous methods, such as the electrochemical MIP sensor, biosensor, and electrochemical colorimetric immunosensor (Sheals et al. 2003; Şengül 2016; Zhang et al. 2017; Xu et al. 2017; Ding et al. 2021), the MIP sensor demonstrates superior sensitivity. This is evident in Table 1.

The LOD achieved in this study is lower than that reported in many other studies and falls below established quality standards. These excellent analytical qualities make the MIP sensor highly valuable for food analysis.

Table 2 Repeatability test results

Characterization method	Current value (μA)				RSD (%) ($n = 4$)
	Day 1	Day 2	Day 4	Day 6	
DPV	3.41	3.46	3.72	3.38	3

Selectivity, repeatability, stability, and recovery test of the MIP sensor

To investigate the MIP electrochemical sensor's ability to detect GLY specifically, potential interferences from pesticides with molecular structures similar to GLY, such as chlorpyrifos and carbendazim, which may be present in the same environment, were tested (Zouaoui et al. 2022; Cahuantzi-Muñoz et al. 2019). As demonstrated in Fig. 7, the current responses of the MIP sensor to GLY were considerably higher than those of the other analogues, indicating that the sensor was capable of preventing interferences and making it more appropriate for selective GLY detection.

The selectivity factor (SF) was then calculated to demonstrate the sensor's high affinity for GLY, according to the following formula:

$$\mathrm{SF} = \mathrm{Slope}_{\mathrm{MIP(Gly)}} / \mathrm{Slope}_{\mathrm{Ana}}. \tag{3}$$

The selectivity factors (SFs) of the MIP sensor for GLY were found to be 27 and 34 times higher than those of the interfering compounds (chlorpyrifos and carbendazim). The low sensitivity observed for both interfering species suggests that the proposed MIP sensor exhibits high selectivity specifically towards GLY.

To assess repeatability, three individual electrodes were prepared under similar conditions on different days, using a GLY concentration of 355 pg/mL. The results, shown in Table 2, indicate a low relative standard deviation (RSD) of 4.3% for the DPV method, demonstrating the reliable repeatability of the MIP sensor for GLY

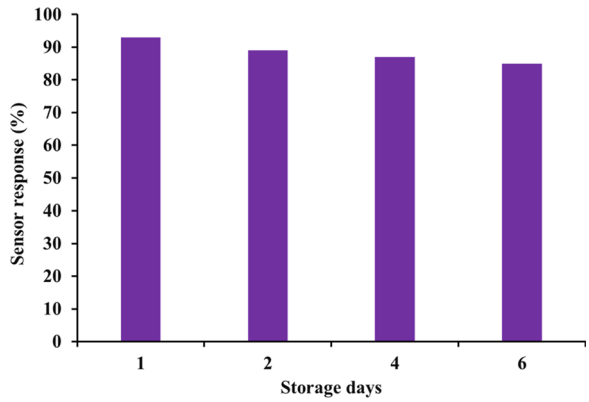

Fig. 8 Investigation of the Stability of the MIP Sensor over a 6-Day Storage Period

detection in surface and agricultural waters. The RSD was calculated using the following formula:

$$\text{RSD} = (\text{Standard Deviation}) * 100/(\text{Mean Signal Value}) \quad (4)$$

Furthermore, the storage stability of the MIP sensor was investigated by periodically measuring its response to a GLY concentration of 355 pg/mL over a span of 1 month. After each measurement, the electrode was thoroughly rinsed with distilled water and stored at 4 °C in 0.01 M PBS (pH = 7.4). The results, presented in Fig. 8, reveal that the sensor maintained 93% of its initial response for 2 days. Subsequently, the response decreased to 85% after 4 days and stabilized at 81% within 6 days, indicating excellent long-term stability.

To assess the reliability of the MIP sensor, a recovery test was conducted by adding different GLY concentrations (273; 355; and 533 pg/mL) to uncontaminated water and cucumber samples. To assess the performance of the MIP sensor, 10 µL of each spiked sample was individually added onto the surface of the sensor. As indicated in Table 3, the recovery rates for the entire solution ranged from 96.05 to 87.75%, with a relative standard deviation (RSD) of less than 5.7%.

Table 3 Results of the recovery test

Samples	Added concentrations (pg/mL)	Found concentrations (pg/mL)	Recovery rate (%)
Tap water	273	251.19	92.01
Cucumber	355	341.00	96.05
Tap water	533	467.74	87.75

Table 4 GLY detection in surface water, agricultural wastewater, agricultural soils and cucumber samples

Samples	Concentration found (pg/mL)	RSD (%) ($n = 3$)
Surface water next to agricultural grain fields	0.001	5.4
Agricultural water	0.003	5.6
Agricultural soils	0.001	2.5
Cucumbers	0.007	2.9

Practical application of the GLY MIP sensor

The developed MIP sensor has been tested for the determination of GLY in contaminated Surface water next to agricultural grain fields, Agricultural water, Agricultural soils, and Cucumbers samples to demonstrate its repeatability in practical applications. During this test, the DPV sensor responses were measured, and the maximum current values of the signal were recorded. The relative difference between the peak current of blank, and the sensor response after exposure to the contaminated samples is inserted into the equation $Y = -3.39\ \text{Log}(C) + 10.24$. The outcomes are summarized in Table 4. Such results provide adequate measurement accuracy, and reliability of the proposed MIP sensor, with acceptable RSDs of less than 5.7%, 4.7%, 4%, 1.6% for agricultural soils, agricultural wastewater, cucumbers, and surface water next to agricultural grain fields, respectively. The GLY content measured in surface waters near agricultural grain fields was 0.001 pg/mL, in agricultural water samples 0.003 pg/mL, in agricultural soils 0.001 pg/mL, and in cucumber samples 0.007 pg/mL.

Conclusion

To summarize, an MIP sensor for detecting GLY has been created by polymerizing methacrylic acid with GLY as a template on a screen-printed carbon electrode. The sensor demonstrated a high linearity and detectability with a low detection limit of 0.001 pg/mL using EIS. Selectivity, repeatability, and recovery tests were satisfactory, making the method accurate, rapid, and cost-effective for detecting low levels of GLY in contaminated surface water near grain fields, agricultural waters, agricultural soils, and cucumber samples. The success of this sensor suggests its potential use in detecting GLY residues in food and other environmental samples.

Author contributions
YA contributed to conceptualization, investigation, formal analysis, validation and writing—original draft. HB contributed to investigation and formal analysis. FS contributed to conceptualization, methodology, and writing—review and editing. BC contributed to writing—review and editing. NEB contributed to conceptualization, visualization, writing—review and editing, and supervision. All authors have read and approved the final version of the manuscript.

Funding
The authors would like to thank the financial support of Moulay Ismail University "Scientific Research Promotion" and CANLEISH under H2020-MSCA-RISE-2020 CANLEISH project (grant agreement 101007653).

Availability of data and materials
Not applicable.

Declarations

Competing interests
The authors declare that they have no competing interests.

Received: 1 September 2023 Accepted: 24 January 2024
Published online: 02 February 2024

References

Aghoutane Y, Diouf A, Österlund L, Bouchikhi B, El Bari N. Development of a molecularly imprinted polymer electrochemical sensor and its application for sensitive detection and determination of malathion in olive fruits and oils. Bioelectrochemistry. 2020;132:107404.
Akin M, Bekmezci M, Bayat R, Coguplugil ZK, Sen F, Karimi F, et al. Mobile device integrated graphene oxide quantum dots based electrochemical biosensor design for detection of miR-141 as a pancreatic cancer biomarker. Electrochim Acta. 2022;435:141390.
Arikan K, Burhan H, Bayat R, Sen F. Glucose nano biosensor with non-enzymatic excellent sensitivity prepared with nickel–cobalt nanocomposites on f-MWCNT. Chemosphere. 2022;291:132720.
Bakas I, Ben Oujji N, Moczko E, Istamboulie G, Piletsky S, Piletska E, et al. Molecular imprinting solid phase extraction for selective detection of methidathion in olive oil. Anal Chim Acta. 2012;734:99–105.
Bayat R, Bekmezci M, Akin M, Isik I, Sen F. Nitric oxide detection using a corona phase molecular recognition site on chiral single-walled carbon nanotubes. ACS Appl Bio Mater. 2023. https://doi.org/10.1021/acsabm.3c00573.
Blanco-López M, Lobo-Castañón M, Miranda-Ordieres A, Tuñón-Blanco P. Voltammetric sensor for vanillylmandelic acid based on molecularly imprinted polymer-modified electrodes. Biosens Bioelectron. 2003;18(4):353–62.
Blanco-López MC, Lobo-Castañón MJ, Miranda-Ordieres AJ, Tuñón-Blanco P. Electrochemical sensors based on molecularly imprinted polymers. TrAC Trends Anal Chem. 2004;23(1):36–48.
Bou-Mitri C, Mekanna AN, Dagher S, Moukarzel S, Farhat A. Occurrence and exposure to glyphosate present in bread and flour products in Lebanon. Food Control. 2022;136:108894.
Bukowska B, Woźniak E, Sicińska P, Mokra K, Michałowicz J. Glyphosate disturbs various epigenetic processes in vitro and in vivo: a mini review. Sci Total Environ. 2022;851:158259.
Bus JS. Analysis of moms across America report suggesting bioaccumulation of glyphosate in U.S. mother's breast milk: implausibility based on inconsistency with available body of glyphosate animal toxicokinetic, human biomonitoring, and physico-chemical data. Regul Toxicol Pharmacol. 2015;73(3):758–64.
Cahuantzi-Muñoz SL, González-Fuentes MA, Ortiz-Frade LA, Torres E, Țălu Ș, Trejo G, et al. Electrochemical biosensor for sensitive quantification of glyphosate in maize kernels. Electroanalysis. 2019;31(5):927–35. https://doi.org/10.1002/elan.201800759.
Campanile R, Elia VC, Minopoli A, Ud Din Babar Z, di Girolamo R, Morone A, et al. Magnetic micromixing for highly sensitive detection of glyphosate in tap water by colorimetric immunosensor. Talanta. 2023;253:123937.
Campbell G, Mannetje A, Keer S, Eaglesham G, Wang X, Lin C-Y, et al. Characterization of glyphosate and AMPA concentrations in the urine of Australian and New Zealand populations. Sci Total Environ. 2022;847:157585.
Cao Y, Wang L, Wang C, Hu X, Liu Y, Wang G. Sensitive detection of glyphosate based on a Cu-BTC MOF/g-C_3N_4 nanosheet photoelectrochemical sensor. Electrochim Acta. 2019;317:341–7.
Cederlund H. Environmental fate of glyphosate used on Swedish railways: results from environmental monitoring conducted between 2007–2010 and 2015–2019. Sci Total Environ. 2022;811:152361.
Chen L, Wang X, Lu W, Wu X, Li J. Molecular imprinting: perspectives and applications. Chem Soc Rev. 2016;45(8):2137–211.
Clermont-Paquette A, Mendoza D-A, Sadeghi A, Piekny A, Naccache R. Ratiometric sensing of glyphosate in water using dual fluorescent carbon dots. Sensors. 2023;23(11):5200. https://doi.org/10.3390/s23115200.
Cui Y, Ding J, Su Y, Ding L. Facile construction of magnetic hydrophilic molecularly imprinted polymers with enhanced selectivity based on dynamic non-covalent bonds for detecting tetracycline. Chem Eng J. 2023;452:139291.
da Silva AS, Fernandes FCB, Tognolli JO, Pezza L, Pezza HR. A simple and green analytical method for determination of glyphosate in commercial formulations and water by diffuse reflectance spectroscopy. Spectrochim Acta Part A Mol Biomol Spectrosc. 2011;79(5):1881–5.
de Oliveira MA, da Gonzaga MLC, Araújo BS, Furtado RF, Muniz CR, Ayala AP, et al. Synthesis of poly (methacrylic acid-co-ethylene glycol methacrylate) as a molecularly printed polymer for histamine detection. Chem Pap. 2023;77(4):1821–33. https://doi.org/10.1007/s11696-022-02537-x.
Ding S, Lyu Z, Li S, Ruan X, Fei M, Zhou Y, et al. Molecularly imprinted polypyrrole nanotubes based electrochemical sensor for glyphosate detection. Biosens Bioelectron. 2021;191:113434.
Diouf A, Motia S, El Hassani NEA, El Bari N, Bouchikhi B. Development and characterization of an electrochemical biosensor for creatinine detection in human urine based on functional molecularly imprinted polymer. J Electroanal Chem. 2017;788:44–53.
Diouf A, Moufid M, Bouyahya D, Österlund L, El Bari N, Bouchikhi B. An electrochemical sensor based on chitosan capped with gold nanoparticles combined with a voltammetric electronic tongue for quantitative aspirin detection in human physiological fluids and tablets. Mater Sci Eng C. 2020;110:110665.
Do MH, Florea A, Farre C, Bonhomme A, Bessueille F, Vocanson F, et al. Molecularly imprinted polymer-based electrochemical sensor for the sensitive detection of glyphosate herbicide. Int J Environ Anal Chem. 2015;95(15):1489–501. https://doi.org/10.1080/03067319.2015.1114109.
Gandhi K, Khan S, Patrikar M, Markad A, Kumar N, Choudhari A, et al. Exposure risk and environmental impacts of glyphosate: highlights on the toxicity of herbicide co-formulants. Environ Chall. 2021;4:100149.
Gillezeau C, van Gerwen M, Shaffer RM, Rana I, Zhang L, Sheppard L, et al. The evidence of human exposure to glyphosate: a review. Environ Heal. 2019;18(1):2. https://doi.org/10.1186/s12940-018-0435-5.
Hori Y, Fujisawa M, Shimada K, Hirose Y. Determination of the herbicide glyphosate and its metabolite in biological specimens by gas chromatography-mass spectrometry. A case of poisoning by roundup(r) herbicide. J Anal Toxicol. 2003;27(3):162–6. https://doi.org/10.1093/jat/27.3.162.
Jiang J, Lucy C. Determination of glyphosate using off-line ion exchange preconcentration and capillary electrophoresis-laser induced fluorescence detection. Talanta. 2007;72(1):113–8.
Kalofiri P, Balias G, Tekos F. The EU endocrine disruptors' regulation and the glyphosate controversy. Toxicol Rep. 2021;8:1193–9.
Kodama S, Ito Y, Taga A, Nomura Y, Yamamoto A, Chinaka S, et al. A fast and simple analysis of glyphosate in tea beverages by capillary electrophoresis with on-line copper(II)-glyphosate complex formation. J Heal Sci. 2008;54(5):602–6.
Kronberg MF, Rossen A, Munarriz ER. Glyphosate-based herbicides and oxidative stress. In: Toxicology. Elsevier; 2021. pp. 79–90. https://linkinghub.elsevier.com/retrieve/pii/B9780128190920000091
Lanzarin GAB, Venâncio CAS, Félix LM, Monteiro SM. Evaluation of the developmental effects of a glyphosate-based herbicide complexed with copper, zinc, and manganese metals in zebrafish. Chemosphere. 2022;308:136430.

Lares BA, Vignatti AM, Echaniz SA, Gutiérrez MF. Effects of glyphosate on cladocera: a synthetic review. Aquat Toxicol. 2022;249:106232.
Li S, Pilla S, Gong S. Modulated molecular recognition by a temperature-sensitive molecularly-imprinted polymer. J Polym Sci Part A Polym Chem. 2009;47(9):2352–60. https://doi.org/10.1002/pola.23325.
Li Y, Zhang S, Zhang Q, Xu G, Dai H, Lin Y. Binding-induced internal-displacement of signal-on photoelectrochemical response: a glyphosate detection platform based on graphitic carbon nitride. Sensors Actuators B Chem. 2016;224:798–804.
Liu H, Chen P, Liu Z, Liu J, Yi J, Xia F, et al. Electrochemical luminescence sensor based on double suppression for highly sensitive detection of glyphosate. Sensors Actuators B Chem. 2020;304:127364.
Madani NA, Carpenter DO. Effects of glyphosate and glyphosate-based herbicides like Roundup™ on the mammalian nervous system: a review. Environ Res. 2022;214:113933.
Maddalon A, Galbiati V, Colosio C, Mandić-Rajčević S, Corsini E. Glyphosate-based herbicides: evidence of immune-endocrine alteration. Toxicology. 2021;459:152851.
Melton LM, Taylor MJ, Flynn EE. The utilisation of ion chromatography and tandem mass spectrometry (IC-MS/MS) for the multi-residue simultaneous determination of highly polar anionic pesticides in fruit and vegetables. Food Chem. 2019;298:125028.
Motojyuku M, Saito T, Akıeda K, Otsuka H, Yamamoto I, Inokuchi S. Determination of glyphosate, glyphosate metabolites, and glufosinate in human serum by gas chromatography–mass spectrometry. J Chromatogr B. 2008;875(2):509–14.
Ngai KS, Ramesh S, Ramesh K, Juan JC. A review of polymer electrolytes: fundamental, approaches and applications. Ionics (Kiel). 2016;22(8):1259–79. https://doi.org/10.1007/s11581-016-1756-4.
Rong Q, Han H, Feng F, Ma Z. Network nanostructured polypyrrole hydrogel/Au composites as enhanced electrochemical biosensing platform. Sci Rep. 2015;5(1):11440.
Sanchez Martín MJ, Villa MV, Sánchez-Camazano M. Glyphosate-hydrotalcite interaction as influenced by pH. Clays Clay Miner. 1999;47:777–83. https://doi.org/10.1346/CCMN.1999.0470613.
SekliBelaïdi F, Farouil L, Salvagnac L, Temple-Boyer P, Séguy I, Heully JL, et al. Towards integrated multi-sensor platform using dual electrochemical and optical detection for on-site pollutant detection in water. Biosens Bioelectron. 2019;132:90–6.
Şengül Ü. Comparing determination methods of detection and quantification limits for aflatoxin analysis in hazelnut. J Food Drug Anal. 2016;24(1):56–62.
Sheals J, Granström M, Sjöberg S, Persson P. Coadsorption of Cu(II) and glyphosate at the water–goethite (α-FeOOH) interface: molecular structures from FTIR and EXAFS measurements. J Colloid Interface Sci. 2003;262(1):38–47.
Soares D, Silva L, Duarte S, Pena A, Pereira A. Glyphosate use, toxicity and occurrence in food. Foods. 2021;10(11):2785.
Tarannum N, Khatoon S, Sharma MK. Computational approach to establish molecularly imprinted polymers interaction of functional monomer methacrylic acid and template norfloxacin. Comput Theor Chem. 2023;1224:114124.
Weisenburger DD. A review and update with perspective of evidence that the herbicide glyphosate (roundup) is a cause of non-hodgkin lymphoma, clin. Clin Lymphoma Myeloma Leuk. 2021;21(9):621–30.
Xu J, Zhang Y, Wu K, Zhang L, Ge S, Yu J. A molecularly imprinted polypyrrole for ultrasensitive voltammetric determination of glyphosate. Microchim Acta. 2017;184(7):1959–67. https://doi.org/10.1007/s00604-017-2200-9.
Xu J, Smith S, Smith G, Wang W, Li Y. Glyphosate contamination in grains and foods: an overview. Food Control. 2019;106:106710.
Yuan Y, Jiang J, Liu S, Yang J, Zhang H, Yan J, et al. Fluorescent carbon dots for glyphosate determination based on fluorescence resonance energy transfer and logic gate operation. Sensors Actuators B Chem. 2017;242:545–53.
Zhang C, She Y, Li T, Zhao F, Jin M, Guo Y, et al. A highly selective electrochemical sensor based on molecularly imprinted polypyrrole-modified gold electrode for the determination of glyphosate in cucumber and tap water. Anal Bioanal Chem. 2017;409(30):7133–44. https://doi.org/10.1007/s00216-017-0671-5.
Zhao T, Guan X, Tang W, Ma Y, Zhang H. Preparation of temperature sensitive molecularly imprinted polymer for solid-phase microextraction coatings on stainless steel fiber to measure ofloxacin. Anal Chim Acta. 2015;853:668–75.
Zouaoui F, Bourouina-Bacha S, Bourouina M, Zine N, Errachid A, Jaffrezic-Renault N. Mathematical modelling of glyphosate molecularly imprinted polymer-based microsensor with multiple phenomena. Molecules. 2022;27(2):493.

Publisher's Note